ADVANCED MATERIALS
www.advmat.de

Biohybrid Variable-Stiffness Soft Actuators that Self-Create Bone

*Danfeng Cao, Jose G. Martinez, Emilio Satoshi Hara, and Edwin W. H. Jager**

Inspired by the dynamic process of initial bone development, in which a soft tissue turns into a solid load-bearing structure, the fabrication, optimization, and characterization of bioinduced variable-stiffness actuators that can morph in various shapes and change their properties from soft to rigid are hereby presented. Bilayer devices are prepared by combining the electromechanically active properties of polypyrrole with the compliant behavior of alginate gels that are uniquely functionalized with cell-derived plasma membrane nanofragments (PMNFs), previously shown to mineralize within 2 days, which promotes the mineralization in the gel layer to achieve the soft to stiff change by growing their own bone. The mineralized actuator shows an evident frozen state compared to the movement before mineralization. Next, patterned devices show programmed directional and fixated morphing. These variable-stiffness devices can wrap around and, after the PMNF-induced mineralization in and on the gel layer, adhere and integrate onto bone tissue. The developed biohybrid variable-stiffness actuators can be used in soft (micro-) robotics and as potential tools for bone repair or bone tissue engineering.

1. Introduction

Variable stiffness is an important property in both nature and human-made devices. Low rigidity and material compliance are required to reduce mechanical resistance or promote morphological adaptation, whereas a high rigidity is required for structural load-bearing after the shape change is complete. A well-known example is the fontanelle structure of the mammalian embryonic skull. The fontanelles allow the skull to temporarily deform during birth to enable the infant's head to pass through the narrow birth canal. After birth, this flexibility is no longer needed, but instead a rigid state is desired to protect the sensitive brain, and thus the material properties of the skull change, closing the skull into a rigid bone. Likewise, variable-stiffness components are of great interest to achieve morphing robotics and in bionics.[1,2] In medicine and tissue engineering, variable stiffness is also of fundamental importance, especially when interacting with the surrounding microenvironment. For instance, compliant hydrogels and scaffolds can be used to facilitate insertion and adaptation during surgery, and thereafter the transplanted materials harden to reconstruct the function and mechanical properties of the injured hard tissue.[2,3]

A number of variable-stiffness actuators have been developed, but they mainly combine components with different stiffness and non-dynamic properties.[2,4] Novel functional materials are decisive for the development of new variable-stiffness systems and functionality. Bioinspired and biohybrid materials that integrate biological components[5] (e.g., cells, enzymes, phospholipids) would enable the development of unprecedented variable-stiffness systems and functionality.

We here report a biohybrid variable-stiffness actuator that creates its own bone. The biohybrid actuator uses the electroactive polymer Polypyrrole (PPy) as the mechanically active component and is combined with alginate (Alg) hydrogels functionalized with cell-derived plasma membrane nanofragments (PMNFs) as the bioinducing source for mineralization and stiffening of the gel layer. This allows the development of unique soft-to-hard variable-stiffness actuators for potential applications in soft (micro-)robotics and bone tissue engineering (**Figure 1**). PMNFs were shown to be the nucleation sites for bone formation in vivo.[6] PMNFs comprise phospholipids and bone formation-related enzymes, including tissue non-specific alkaline phosphatase (TNALP), which promote the hydrolysis of phosphate-containing substrates and release free phosphate ions that further participate in the formation of calcium-phosphate minerals [e.g., amorphous calcium phosphate (ACP), hydroxyapatite (HAp)].[7] Previous reports also demonstrated the ability of the PMNFs to promote rapid mineralization in vitro in just 2 to 3 days,[6,8] while live cells or recombinant TNALP require at least 2 to 3 weeks.[9] The PMNFs are assumed to maintain the membrane-bound enzymes and proteins

D. Cao, J. G. Martinez, E. W. H. Jager
Sensor and Actuator Systems
Department of Physics, Chemistry and Biology (IFM)
Linköping University
Linköping 58183, Sweden
E-mail: edwin.jager@liu.se
E. S. Hara
Department of Biomaterials
Graduate School of Medicine, Dentistry and Pharmaceutical Sciences
Okayama University
Okayama 700–8558, Japan
The ORCID identification number(s) for the author(s) of this article can be found under https://doi.org/10.1002/adma.202107345.

DOI: 10.1002/adma.202107345

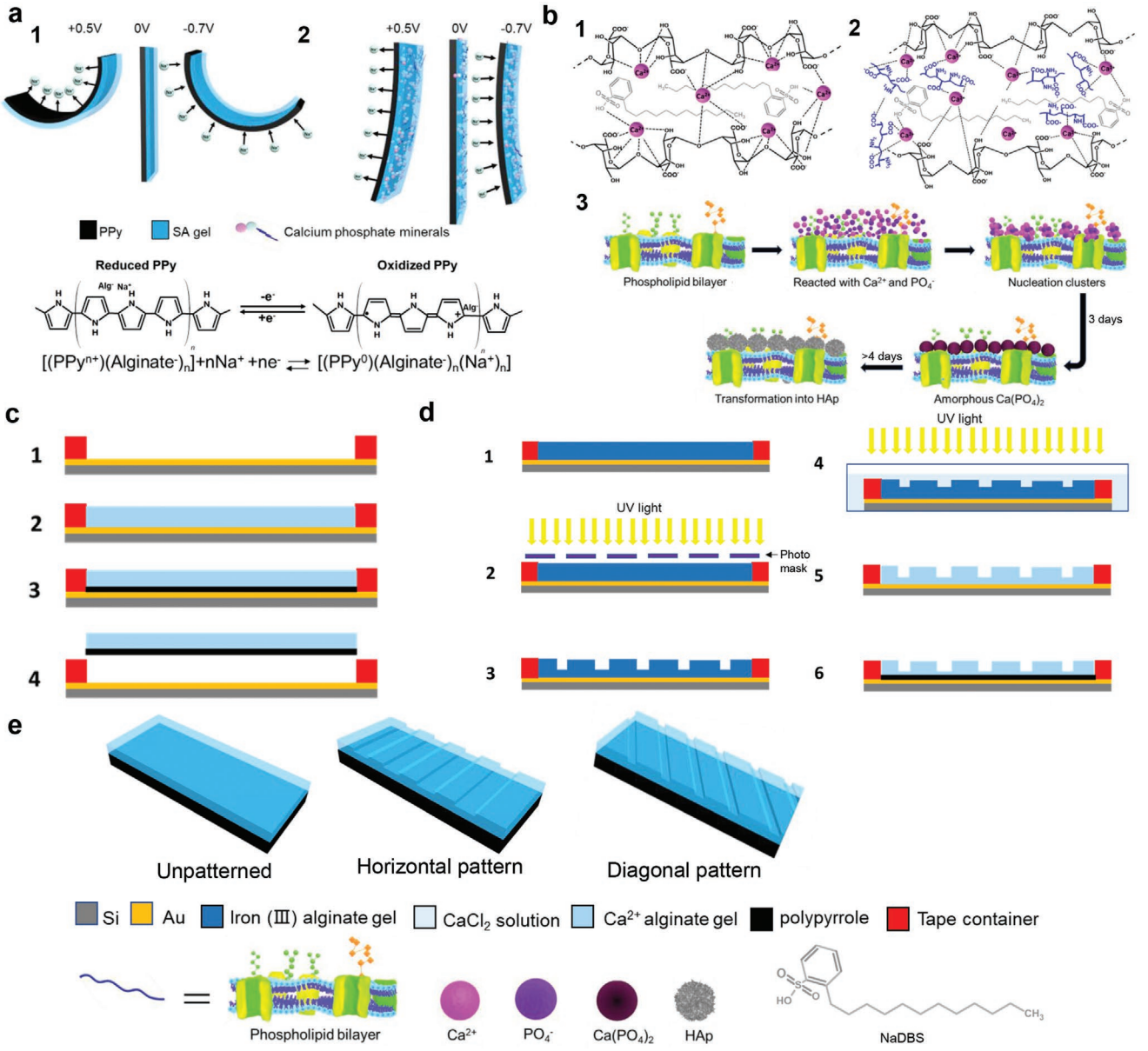

Figure 1. Actuation principle of PPy-Alg and PPy-Alg-PMNF actuators, Alg crosslinking, PMNF mineralization principle, and fabrication of PPy-Alg and PPy-Alg-PMNF actuators. a) Schematic illustration of the electrochemical behavior of PPy-Alg actuator without (1) and with (2) PMNFs. After incubation in mineralizing medium (DMEM), PMNFs induced the formation of calcium phosphate minerals (amorphous calcium phosphate, ACP; hydroxyapatite, HAp), which promoted the stiffening of the Alg gel layer and consequent attenuation of the actuator's mobility. b) Schematic illustration describing the possible crosslinking of the Alg gel (black) without (1) and with (2) PMNFs (blue). Schematic illustration of PMNF mineralization with the formation of ACP and HAp after 3 and 7 days of incubation in DMEM, respectively (3). c) Schematic illustration describing the fabrication procedure of the unpatterned PPy-Alg actuator. 1) Formation of a mold using insulating tape onto an Au/Si substrate. 2) Deposition of sodium Alg solution (with and without PMNFs) and gelification in $CaCl_2$ solution. 3) Electrosynthesis of PPy layer inside the Alg gel. 4) Peeling of PPy-Alg actuator. d) The fabrication process of the patterned PPy-Alg actuators. 1) Drop-casting of sodium Alg gel with iron (III) (Fe^{3+}). 2) Photolithographic patterning of the Alg gel using UV light. 3) Development of the pattern in the Alg gel with Fe^{3+}. 4) Ion exchange of the Fe^{3+} using $CaCl_2$ solution under UV light. 5) Crosslinking of the patterned Alg gel by Ca^{2+}. 6) Electrosynthesis of PPy layer inside the Alg gel. e) Illustration of the unpatterned and patterned PPy-Alg actuators.

immobilized in their natural state, allowing their optimal activity, and thus PMNFs would be a key component of novel functional biohybrid materials.

Here, we use a bilayer actuator, comprising PPy and Alg layers, but other actuator configurations, for example, linear, are of course possible. The actuation is based on the electrochemically induced volume change of PPy due to the exchange of ions and solvent into the polymer matrix through reversible oxidation and reduction reactions.[10] When PPy doped with large immobile anions (Alg in this case) is reduced, the amount of positive charges on the PPy chains decreases and cations (Na^+) and solvent, enter the PPy matrix to maintain

the overall charge neutrality and the osmotic pressure respectively, leading to an increase of the PPy volume. Reversing the applied potential, that is, oxidizing PPy, results in the opposite behavior: the Na^+ cations and solvent are expelled to maintain the charge neutrality, causing the PPy to contract. This volume change is used to make soft actuators, or artificial muscles, in various configurations[10b,11] and applications, such as microrobotics[12] and micro-unmanned aerial vehicles.[13] By attaching PPy to a passive layer the reversible volume change is converted into a bending motion (Figure 1a-1). We chose Alg as the passive layer in the bilayer actuator since it is soft, frequently used in tissue engineering, and allows functionalization with biomolecules. PMNFs were immobilized in the Alg hydrogel as the bioactive component. Upon incubation in a medium rich in phosphate-containing substrates and calcium, the PMNFs induce rapid mineralization in the gel, making it mechanically rigid and thus reducing the actuator movement (Figure 1a-2).

2. Results

First, we fabricated plain PPy-Alg bilayer actuators (Figure 1c), that is, without any PMNFs, investigated their performance and optimized the PPy-Alg thickness ratio (Figures S1–S4, Table S1, Supporting Information). The actuators bent upon switching the applied potential, following the typical cation (Na^+) driven mechanism volume change, as expected from PPy with the large Alg molecules acting as immobile counterions.[10b,14,15] During reduction PPy swelled, bending the actuator towards the gel direction, and vice-versa, during the oxidation, PPy contracted and the actuator to bent towards the PPy side. The 70C actuator showed a bending of almost 90°, or 26 mm, at –0.7 V. The total thickness of the bilayer was ≈340 μm, of which PPy was 170 μm, compared to ≈313 μm for the native Alg gel, indicating that PPy was synthesized both inside and partially outside the Alg gel, which also improves the mechanical adhesion between the two layers.[16,17]

2.1. Bioinduced Variable Stiffness

Next, we functionalized the Alg gel with the PMNFs to fabricate the soft-to-hard variable-stiffness PPy-Alg-PMNF actuators and investigated their performance. Figure S5, Supporting Information, shows the bending displacements of PPy-Alg-PMNF and PPy-Alg (without PMNFs) actuators. The two actuators show similar movement (30 mm vs 26 mm during the last cycle, respectively) indicating that the immobilization of the PMNFs in the Alg gel did not affect the actuation.

The PPy-Alg-PMNF actuators were then incubated for 3, 5, or 7 days in Dulbecco's modified Eagle medium (DMEM) to promote PMNF-induced mineralization in the gel layer or in 0.1 M NaCl solution as the control medium. After incubation, they were all actuated in 0.1 M NaCl solution. **Figure 2** shows the movement of the PPy-Alg-PMNF actuator after the various incubation periods in both DMEM and NaCl. Interestingly, the movement of PPy-Alg-PMNF actuator was reduced significantly after 3 days of incubation in DMEM, and completely blocked after incubation for 5 days or longer (Figure 2a,c). We attribute this to the increasing formation of minerals in the gel layer of the actuator, making the gel stiffer and thus restricting and finally impeding the movement (Figure S6, Supporting Information). When incubated in the control solution NaCl, which means that no mineralization could occur, the PPy-Alg-PMNF actuators still moved normally upon application of the potential (Figure 2b,d).

To confirm that the variable stiffness is indeed caused by the bioinduced mineralization, PPy-Alg-PMNF and PPy-Alg actuators were actuated in both DMEM and NaCl solutions (Figure S7, Supporting Information). When the actuators were incubated in 0.1 M NaCl solution, the PPy-Alg-PMNF actuator presented similar displacement compared to the PPy-Alg actuator. As before, when incubated in DMEM for 3 days the bending displacement of the PPy-Alg-PMNF actuator was markedly suppressed (Figure S7-a, S7-c, Supporting Information), while the displacement of the PPy-Alg actuator was still significant (1.5 mm), although reduced to approximately a tenth. We attribute this latter reduction to the binding and clustering of proteins present in the DMEM to the gel layer, but not to gel calcification, as the detected amount of calcium and phosphorus was substantially low (**Figure 3**a). The presence of calcium in DMEM could enhance the crosslinking of the Alg gel too, contributing to its stiffness increase. The incubation of the PPy-Alg actuator for 3, 5, and 7 days resulted in similar displacements (Figure S8, Supporting Information).

To confirm the formation of minerals in the gel layer, an scanning electron microscopy (SEM)-based structural analysis and energy-dispersive X-ray spectroscopy (EDX)- and X-ray diffraction (XRD)-based qualitative analysis of the PMNF-formed minerals were performed (Figure 3). The formation of minerals was only detected in the PPy-Alg-PMNF gels incubated in DMEM (Figure 3a). The initial minerals were identified to be ACP (Figure 3c), with an average diameter of 84.0 nm ± 12.9 nm (Figure 3b). After incubation for 7 days, the minerals were identified to be crystalline HAp, with an average diameter of 128.3 nm ± 19.7 nm (Figure S9, Supporting Information). Electron diffraction analysis of the minerals using a transmission electron microscope was also performed to confirm the formation of ACP and HAp, after 3 and 7 days of PMNF incubation in DMEM, respectively (Figure S10, Supporting Information). The presence of the minerals significantly affected the stiffness of the hydrogel, as shown in Figure 3d. The stiffness of the gels increased proportionally with the size of the minerals formed by PMNF mineralization due to longer incubation periods in DMEM (Figure 3d, Figure S9, Supporting Information).

To further demonstrate that stiffness is caused by the mineralization of PMNF in the gel, the PPy-Alg-PMNF actuators were incubated in DMEM with phosphatase inhibitors, known to specifically inhibit the PMNF mineralization, for 3, 5, and 7 days. The actuators after incubation in the DMEM with phosphatase inhibitors showed normal and similar displacement as those before incubation (Figure S11, Supporting Information). Results of SEM and EDX analysis confirmed that no minerals were formed after incubation of the PPy-Alg-PMNF actuator in DMEM with phosphatase inhibitors (Figure S12, Supporting Information).

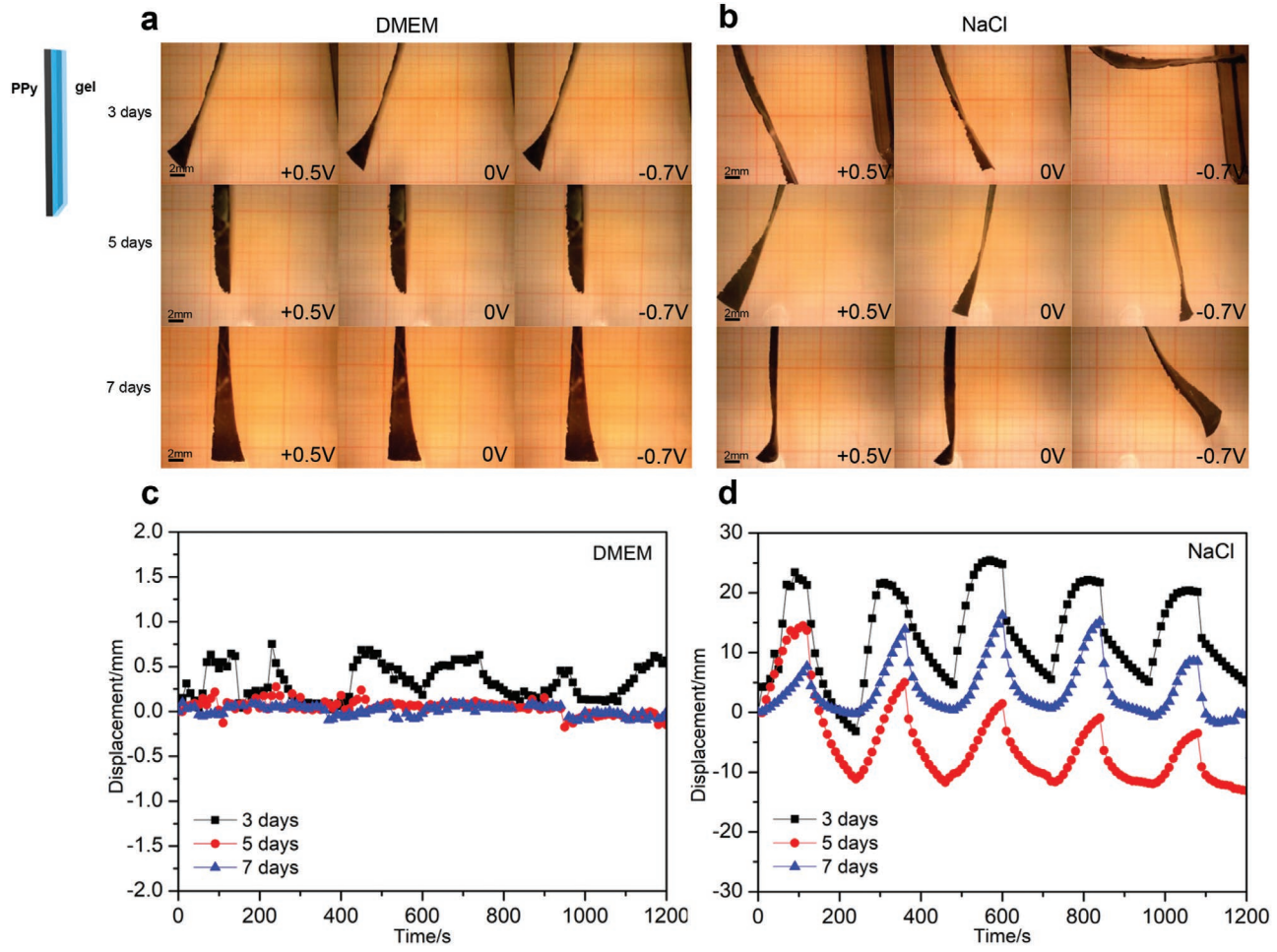

Figure 2. Actuation of PPy-Alg-PMNF actuators after incubation in DMEM or NaCl. a–d) The movement photographs (a,b) and displacement (c,d) of the PPy-Alg-PMNF actuator after incubation in DMEM (a,c) and 0.1 M NaCl (b,d) for 3, 5, 7 days, when activated by applying –0.7 and +0.5 V potential steps (each potential kept for 120 s) in 0.1 M NaCl solution. Note that the bending movement of the PPy-Alg-PMNF actuator was completely blocked after incubation in DMEM for more than 5 days, whilst no changes in the actuator movement were observed when the actuator was incubated in the control 0.1 M NaCl solution.

Figures S13 and S14, Supporting Information, show the electrochemical characterization of the PPy-Alg-PMNF and PPy-Alg actuators after the various incubation periods in both incubation solutions. As can be seen, the actuators remained electrochemically active after all incubations, meaning that the reduced/blocked movement of the PPy-Alg-PMNF actuators is mainly a mechanical effect due to the increased stiffness. The PPy-Alg actuation charge was similar after incubation in both DMEM and NaCl, except for after 5 days of incubation. A decrease in the actuation charge for the PPy-Alg-PMNF actuators could be seen (Figure S15, Supporting Information), from ≈320 mC in NaCl to 170–100 mC in DMEM. Since the displacement of bending bilayers depends linearly on the consumed actuation charge,[18] this means that we should have seen a ≈1/2 to ≈1/3 decrease in the movement and not a complete blockage as we did observe. These results further support that the major contribution to the decrease/blockage of the actuation of the PPy-Alg-PMNF actuator comes from the bone formation in the gel layer. We attribute the reduction of the consumed actuation charge after incubation in DMEM to the fact that PPy is synthesized into the Alg-PMNF gel and that thereby the minerals are also formed in the PPy layer, thus reducing the ion diffusion properties of PPy and the mobility of the PPy chains. Indeed, cross-sectional SEM images revealed three different layers in the PPy-Alg-PMNF actuator: a PPy layer with the conventional cauliflower structure, a hybrid PPy layer close to the Alg gel composed of PPy, minerals, and Alg, and the Alg gel layer with minerals (Figure S16, Supporting Information). The synthesis of PPy partially into the Alg gel layer, forming the hybrid PPy layer, is expected to enhance its adhesion to the gel layer and reduce delamination due to the strain mismatch between layers with different mechanical properties.[19]

2.2. Patterned PPy-Alg-PMNF Actuators

To enhance the functionality of the bilayer actuators and be able to actively direct their movement, we embedded the Alg gel layers with a directional topographic pattern using photolithography,[20] both perpendicular (90°) and diagonally (≈45°)

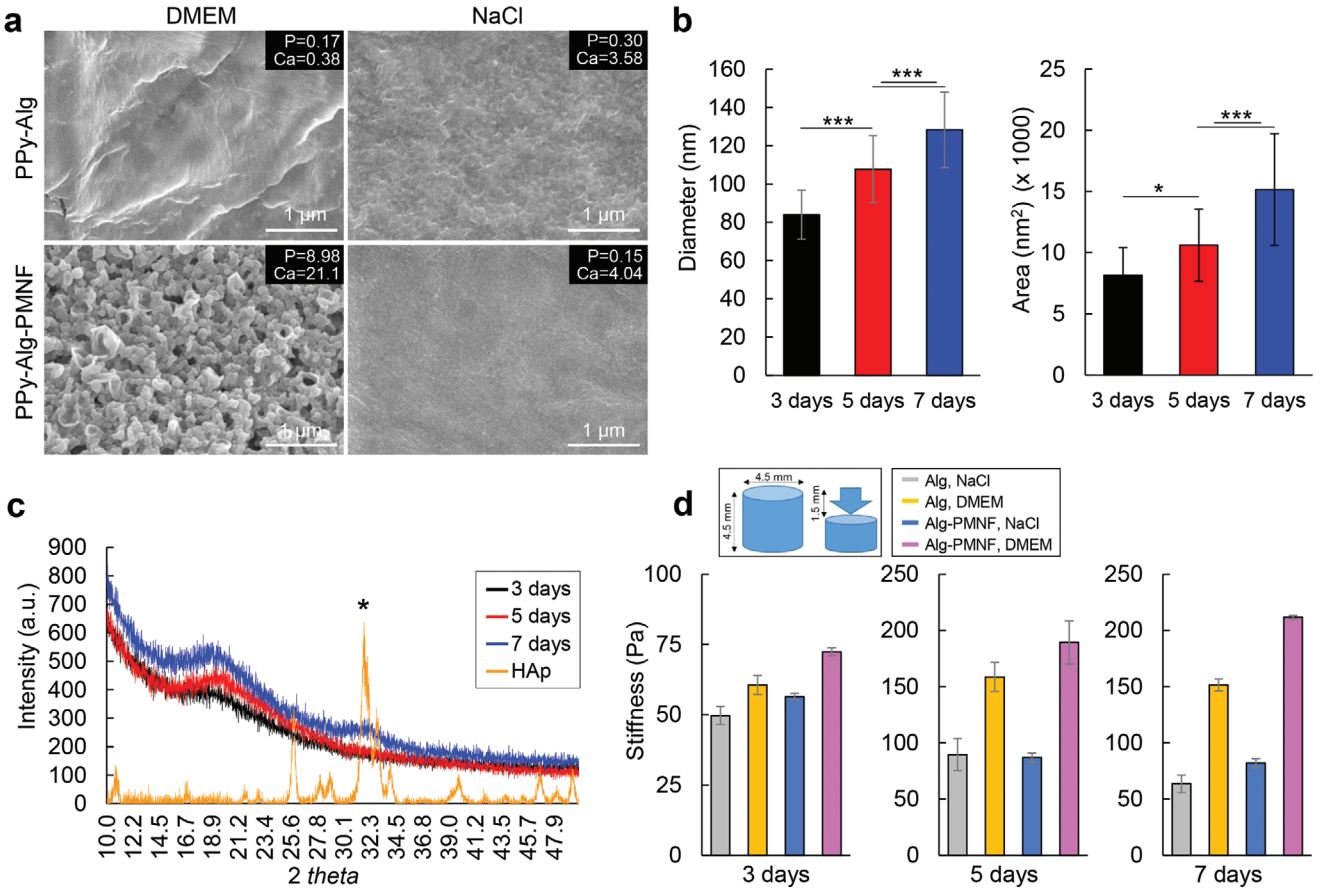

Figure 3. Morphological and mechanical characterization of PPy-Alg and PPy-Alg-PMNF actuators after incubation in DMEM or NaCl. a) SEM images of the gel layer of freeze-dried PPy-Alg and PPy-Alg-PMNF actuators after incubation in DMEM solution or 0.1 M NaCl for 3 days. The insets show the percentage of phosphorus (P) and calcium (Ca) ions detected by EDX. Note the presence of minerals and high levels of P and Ca ions only in the PPy-Alg-PMNF gel incubated in DMEM (left lower panel). b) Graphs showing the quantitative analysis of the diameter and area of the minerals formed in Alg-PMNFs after 3, 5, or 7 days of incubation in DMEM. Note the incubation period-dependent increase in the diameter and area of the minerals (N = 25, from at least 2 different images of each condition). *$p \leq 0.05$; ***$p \leq 0.001$; one-way ANOVA, Bonferroni post-hoc test. c) XRD analysis indicating that the initial minerals formed in Alg-PMNF gels incubated in DMEM for up to 5 days were ACP, which then transformed into HAp crystals after 7 days of incubation in DMEM. Note the broad peak at the 31°–33° 2θ region characterizing the 211, 112, and 300 planes of HAp, indicating the low crystallinity of the minerals. Commercially available HAp was used as a control sample. d) Graphs showing the calculated stiffness of Alg gel cylinders with and without PMNF incubated in NaCl solution or DMEM for 3, 5, and 7 days. The inset shows the dimensions of the gel cylinders and the deflection. The graphs show the representative data of three independent experiments, with at least 3 samples in each group (N = 3). No difference was observed in the axial stiffness between the as-prepared Alg and Alg-PMNF gels, and the respective gels incubated in 0.1 M NaCl solution. The stiffness of the Alg-PMNF gels increased in an incubation period-dependent manner. Alg gel incubated in DMEM also became stiff, but no minerals were detected inside or on its surface; proteins and calcium in DMEM could be acting as stiffening agents.

arranged to the length direction of the actuator (Figure 1e). This designed structure controls the bending shape of the bilayer actuator and enables the fabrication of actuators with embedded intelligence, that is, morphological computing. The perpendicular patterned actuator resulted in a semicircle bending (**Figure 4**b1, Figure S17c, Supporting Information), while the diagonal patterned actuator curls in a tendril or corkscrew shape when actuated (Figure 4d1, Figure S17f, Supporting Information). Notably, the actuator also showed some twisting movement together with the bending motion, more clearly seen at the oxidation potential of +0.5V (Figure 4b1). A further optimization of the mechanical properties of the patterned gel, such as by optimizing the UV exposure time to increase the thickness of the pattern and/or increase the stiffness of the gel at those segments, could further reduce the parallel twisting of the actuator.[21] It is also noteworthy that the actuator incubated in NaCl could bend more uniformly than when incubated in DMEM, which could be due to a non-uniform formation of minerals in the Alg-layer.

We now utilize the bioinduced mineralization to fixate and maintain the programmed directional shape without further energy consumption. This fixation is kept even if some spontaneous re-oxidation/reduction might occur and thus eliminates the need to apply a potential to counteract this. We actively kept the PPy-Alg-PMNF actuators in the semicircle and spiral shapes in DMEM for 3 days to mineralize and thus stiffen. After the incubation, the actuation potentials were again applied and the actuators could not move nor recover the initial straight shapes (Figure 4b2,4d2). The programmed shape was maintained due to PMNF mineralization. The mineralized actuators could be taken out of the solution and even then maintained their

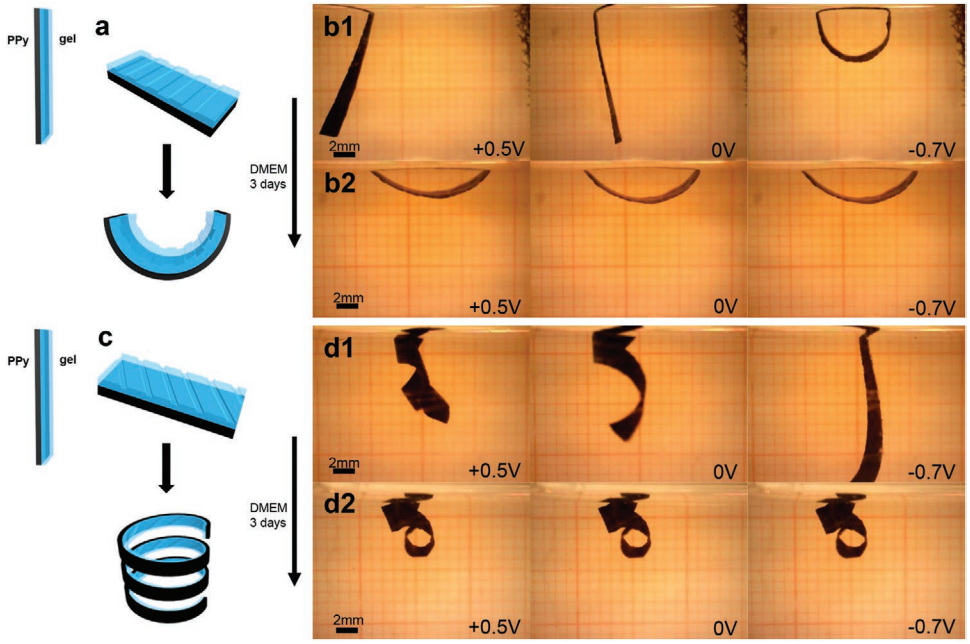

Figure 4. Actuation of patterned PPy-Alg-PMNF actuators before and after incubation. a,c) Schematic design of the perpendicular (a) and diagonally patterned (c) PPy-Alg-PMNF actuators, and their respective bending modes. b,d) Photographs of the perpendicular (b1,b2) and diagonally patterned (d1,d2) PPy-Alg-PMNF actuators' bending movement before (b1, d1) and after (b2, d2) incubation in DMEM for 3 days. All actuation was performed in 0.1 M NaCl.

fixated state, demonstrating that they were also stable in air. This demonstrates that the concept of biological mineralization to form rigid layers can be designed to achieve controllable morphing structures that can be fixated in a final, predetermined shape. This method could be viewed as a bioinduced variant of so-called 4D manufacturing.[22] Current 4D manufacturing methods use external stimuli, such as heat or UV light to modify the object's structure or stiffness, but here we use only Ca^{2+} and PO_4^- to make the structure rigid. This means that the process can be done even where UV light or heat cannot be applied, such as in enclosed environments, remote locations, or once inserted or implanted in the body.

2.3. Morphing and Attaching to Bone

Finally, to demonstrate potential applications in tissue engineering, the PPy-Alg-PMNF actuators were wrapped around a piece of bone to investigate their integration and attachment to bone tissue. First, the horizontally patterned PPy-Alg-PMNF actuators were induced to morph to the bone shape by actuating them in 0.1 M NaCl solution (reduced state). Next, while maintaining wrapped around the bone, they were incubated in either DMEM or 0.1 M NaCl solution for 3 days (**Figure 5**a,b). After the incubation period, the PPy-Alg-PMNF actuators were actuated to assess their adhesiveness to the bone surface. When trying to actuate the PPy-Alg-PMNF actuator after incubation in DMEM, it showed no significant deformation, as before, due to the stiffening of the gel, and it also remained attached to the bone. When the actuator was peeled off by force, parts of the gel remained attached to the bone, and more interestingly, minerals formed in the gel layer were integrated onto the bone surface, as can be seen by the SEM images of the bone surface (Figure 5c). On the other hand, the PPy-Alg-PMNF actuator incubated in NaCl could move effortlessly, separating from the bone, showing no attachment, and leaving no remnants on the bone surface (Figure 5d). This shows that the mineralization that occurred during the incubation of PPy-Alg-PMNF in DMEM initiated the adhesion to the bone, while no mineralization occurred in NaCl incubation. Manually wrapping the PPy-Alg-PMNF actuators more tightly to the bone showed even better adhesion (Figure S18, Supporting Information).

Future in vitro and in vivo studies involving the analysis of chemical, physical, and biological interfacial interactions with living cells would be necessary to further clarify the biocompatibility of the PPy-Alg-PMNF actuators. Notably, the individual elements (i.e., PPy and Alg gel) constituting these biohybrid actuators have already been shown to have high biocompatibility both in vitro and in vivo.[23] Also, for bone tissue engineering applications it is important to optimize the strength of the newly formed bone so that it matches the strength and load bearing properties of the existing bone, that is, is not stronger or weaker.

Moreover, for better control of the actuator's movement a feedback control system could be employed using either integrated strain sensors[24] or analysis of the electrochemical signal during motion.[15,25] Multiscale modeling, including mechanical, electrochemical, and electronic, would further aid actuator design and prediction of movement.[26]

3. Conclusion

We introduced the new concept of bioinduced variable-stiffness actuators that can morph in various, pre-programmed shapes

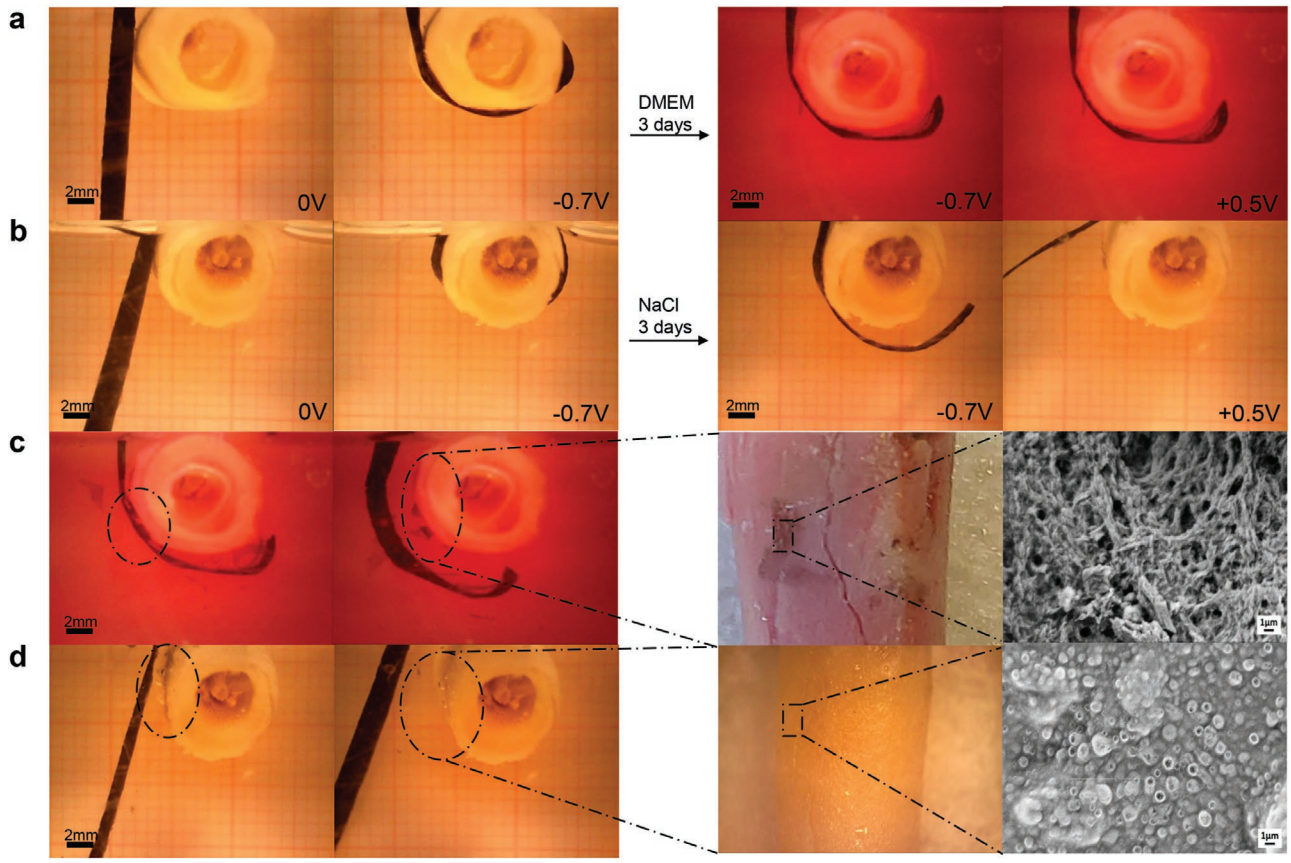

Figure 5. Morphing and integration of PPy-Alg-PMNF actuators around the bone. The morphing of PPy-Alg-PMNF actuators around the bone in 0.1 M NaCl, followed by incubation in a) DMEM or b) NaCl for 3 days. Displacements before (left) and after (right) incubation of PPy-Alg-PMNF actuator when potential steps between +0.5 and −0.7 V were applied. The attachment of PPy-Alg-PMNF actuators to the bone was assessed by peeling off the actuator. The actuator incubated in c) DMEM remained morphed and attached to the bone. Note also that part of the Alg gel remained attached to the bone surface (middle panel) due to mineralization and integration to the bone surface, as can be seen by the formation of minerals in the SEM image (c). The actuator incubated in d) NaCl could effortlessly return to the original position before incubation and did not show any integration to the bone.

and change their properties from soft to rigid by growing their own bone. We embedded the devices with morphological computing, that is, actuation in a programmed direction, thus enabling fixating the devices in a predetermined shape, without energy consumption, which facilitates their future application in morphing robotics, including as a biohybrid variant of so-called 4D manufacturing. We showed that the devices can be used as morphing biological adhesives, beneficial in future applications such as morphing and integrating around bone fractures, or expanding inside cavities and initiating bone regrowth and related hard-tissue repair.

Here, we used bending actuators to visualize the changed stiffness, but the concept can be extended to other, for example, linear polymeric actuators. PMNFs could be isolated from different cells, with different protein/enzyme expression patterns, which can consequently endow the devices with diverse functionality. Therefore, PMNF-based biohybrid materials could enable the development of novel and unique morphing, phase-changing robotics devices ("Soft-to-Hard robots"). A soft robot being in its embryonic state, cf. jellyfish, could be inserted through a small orifice, for instance, inserted into the body using a syringe, and thereafter unfold, reshape, or morph in its final structure and start growing its own load-bearing components, that is, its bones. PMNF-based biohybrid materials could be used in new tools for tissue engineering, including robot-assisted surgical interventions, such as morphing bioadhesives, to adhere (electronic) components to bone, or to create a hard protective shell around such electronic components that integrates into the body.

4. Experimental Section

Materials: The pyrrole (Py) monomer (Fluka, Switzerland) was vacuum distilled and stored at −20 °C prior to use. Sodium Alginate (NaAlg), calcium chloride dihydrate ($CaCl_2{\cdot}2H_2O$), sodium chloride (NaCl), DMEM, sodium-L-lactate, iron (III) chloride ($FeCl_3$), sodium dodecylbenzenesulfonate (NaDBS), sodium hypochlorite solution (NaClO) (6–14% active chlorine), phosphatase inhibitor cocktail 2, and ethanol were purchased from Sigma-Aldrich (St Louis, MO, USA) and used as received. Lithium perchlorate was purchased from Tokyo Chemical Industry (Tokyo, Japan) and used as received. Ultrapure water (18.2 MΩ) was obtained from Milli-Q Plus water equipment and used for the experiments.

PMNFs were isolated from pre-chondrogenic ATDC5 cells, as reported.[6,8] Briefly, the cells were cultured in 225 cm^2 flasks until confluency, trypsinised, and harvested by centrifugation. A total of 1×10^7 cells in 1 mL of ultrapure water were submitted to ultrasonication

for 3 min for cell fragmentation. PMNFs were then isolated by a series of centrifugation steps at 2000×*g*, 10 000×*g*, and 20 000×*g*, followed by ultracentrifugation at 150 000×*g* for 60 min, based on previous reports.[6,8,27] The amount of PMNFs was determined by the concentration of proteins estimated by the bicinchoninic acid assay (BCA) assay, according to the manufacturer's protocol (Biovision, Milpitas, CA, USA). To induce mineralization of PMNFs, they were incubated in DMEM for up to 7 days. To inhibit the mineralization of PMNFs, they were incubated in DMEM containing phosphatase inhibitors (1:100 dilution).

Preparation of Sodium Alginate Solutions: To obtain 2.5% w/v and 5% w/v sodium alginate (NaAlg) solutions, respective amounts of 1.25 and 2.5 g of NaAlg powder were added into 50 mL of 0.1 M NaDBS solution and mixed under vigorous stirring for 24 h at room temperature. Next, 10 µg of PMNFs was added to 1 mL of the NaAlg/NaDBS solution and mixed for 1 h in an ultrasonic bath to achieve a homogeneous solution. Control samples were prepared without the addition of PMNFs. The prepared solutions were stored at 4 °C.

Preparation of Unpatterned PPy-Alg Actuators: Figure 1c illustrates the fabrication procedure of the PPy-Alg actuator. A piece of silicon (20 mm × 40 mm) was precoated with 30 Å Cr and 1000 Å Au films using thermal evaporation. Electrically insulating tape was fixed at the edges of the Au/Si substrate to form a mold (14 mm × 30 mm). Next, 200 µL of 2.5% NaAlg solution with or without PMNFs was uniformly dropped onto the Au/Si substrate, confined by the tape at the borders, and cross-linked by immediate immersion into 1 M $CaCl_2$ solution for 10 s. Figure 1b illustrates the possible crosslinking mechanism of Alg gel with and without PMNFs. Calcium ions (Ca^{2+}) could crosslink with the COO^- groups in NaAlg and PMNF (blue in Figure 1b) or OH groups in NaDBS (grey in Figure 1b) to form the gel actuator. Thereafter, the PPy was electropolymerized in the Alg gel layer. The Au/Si substrate with the Alg gel film was used as the working electrode, Ag/AgCl (3 M NaCl; model RE-5B from BASi) as the reference electrode, and a stainless steel mesh (30 mm × 70 mm) as the counter electrode, forming a classical three-electrode electrochemical setup. All the potentials in this work were referred to this reference electrode. The three electrodes were immersed into 0.1 M Py in 0.1 M $LiClO_4$ electrolyte to electropolymerize the PPy film at a constant potential (0.7 V) using a potentiostat (IviumStat-XRe, Ivium Technologies, The Netherlands). The electropolymerization was stopped when 50, 70, or 90C charge was consumed. The obtained PPy-Alg actuator layer was then peeled off from the Au/Si substrate and stored in ultrapure water. The thickness of PPy-Alg was measured with a microscope (Carl Zeiss Axioscope A1 HAL100 Microscope, Germany).

Preparation of Patterned PPy-Alg Actuators: An amount of 350 µL of 2.5% NaAlg solution with sodium-L-lactate (175 µL of 5% NaAlg solution without or with PMNFs (10 µg mL^{-1})), 168 µL 0.1 M NaDBS, and 7 µL 500 mM sodium-L-lactate) was uniformly dispensed onto the Au/Si substrate and immediately immersed into 0.1 M $FeCl_3$ solution for 30 s to crosslink the Alg hydrogel. The iron (III)-Alg gel was irradiated through a photolithographic Cr mask using UV light at 2.9 mW cm^{-2} for 6 min using a mask aligner (Carl-Suss MJB3, Garching, Germany). Two patterns, one perpendicular and the other oblique (at about 45°) to the main axis, were fabricated (Figure 1d). The hydrogel was then washed by immersion in 0.9% NaCl solution for 6 min and ultrapure water for 3 min. The resulting patterned iron (III)-crosslinked Alg gel was immersed in a 0.1 M $CaCl_2$ solution and irradiated with UV light of 2.9 mW cm^{-2} intensity in the center for 20 min to exchange the ions.[20] PPy was synthesized in the Alg gel as described in Section 4.3, until 70C charge was consumed. Finally, the obtained patterned PPy-Alg actuator layer was peeled off from the Au/Si substrate and stored in ultrapure water.

Actuation of PPy-Alg Actuators: Electrochemical actuation of the different PPy-Alg actuators was performed in 0.1 M NaCl solution using the same electrochemical setup as described in Section 4.3. A portable USB microscope (Edge, Dino-Lite) was used to record the movement of the actuators. The linear displacement of the tip of the actuator was obtained from the video using a home-programmed Matlab R2017b-based script.

For characterization of the unpatterned PPy-Alg actuators, with or without PMNFs, the following procedures were used: The PPy-Alg actuator (14 mm × 30 mm) was cut in half along the length of the fabricated actuator and incubated for 3, 5, and 7 days; one half in DMEM to induce mineralization and the other half in 0.1 M NaCl solution as the control. After each incubation period, the halves were cut into 2 mm × 25 mm strips and submerged into 0.1 M NaCl electrolyte solution to measure the bending behavior using potential steps of 120s between –0.7 and 0.5 V, for 5 cycles.

For characterization of patterned PPy-Alg actuators, with or without PMNFs, the patterned actuator was cut into 2 mm × 25 mm strips, which were then submerged into 0.1 M NaCl electrolyte solution as described above. The chronoamperometry at –0.7 and 0.5 V was applied for 3 cycles, each potential for 300 s. After these 3 initial bending cycles, the actuator was kept at open circuit to keep a fixed shape and immersed into DMEM for 3 days to induce mineralization. Subsequently, the mineralized actuator was submerged into 0.1 M NaCl electrolyte for measurement of the bending behavior using the same conditions as described above.

Quantitative and Qualitative Characterization of PMNF-Formed Minerals: Analysis of the Alg surface structure with and without PMNFs was performed with SEM, using a Leo1550 Gemini SEM (Zeiss, Germany) at 3 kV, or an S-4800 SEM (Hitachi, Tokyo, Japan) at 5 kV. For the SEM imaging, the samples were incubated in DMEM (to induce mineral formation) or NaCl (control) for 3, 5, or 7 days, washed in ultrapure water, frozen at –80 °C, and vacuum-dried. The samples were then placed onto an aluminum holder and coated with platinum or osmium before SEM observation. Elemental components were evaluated using EDX (Oxford Instruments, UK) with an electron acceleration voltage of 20 kV. Quantitative analysis of mineral area and diameter was performed with image analyzer software ImageJ version 1.53a (NIH, Bethesda, MD, USA).

Qualitative analysis of the minerals formed from PMNF mineralization was performed with an XRD instrument (RINT2500HF, Rigaku Corp., Tokyo, Japan) at an incidence angle of 1° using Cu-Kα (1.54 Å) irradiation at 40 kV and 200 mA. The samples were fixed onto a non-reflecting silicon plate and submitted to XRD measurements, conducted from 10° to 50° at a scan speed of 0.2° min^{-1}. Commercially available HAp was used as the reference sample.

The minerals formed after incubation of PMNFs in DMEM for 3 or 7 days were also observed in a transmission electron microscope (JEM-2100F, JEOL, Tokyo, Japan) operated at 200kV using a current density of 40 pAcm^{-2}. Electron diffraction was also performed at a distance of 60 mm for qualitative analysis of the minerals, according to the methods described previously.[5]

Estimation of the Axial Stiffness of the Gels: Estimation of the axial stiffness of the NaAlg gels was performed with Alg gel cylinders fabricated by cutting out the cylinders from an Alg sheet of 4.5 mm in thickness using a biopsy punch of 4.5 mm in diameter. Details of the preparation of Alg gel sheets have been described elsewhere.[28] Briefly, 2.5% w/v NaAlg solutions, with or without PMNFs, were poured into a porous alumina mold (50 mm × 50 mm × 4.5 mm (H)) and immediately soaked in 1 M calcium chloride solution and maintained for 12 h for complete gelation. The gel sheets (4.5 mm in thickness) were then washed in 0.1 M NaCl solution and used for fabrication of the gel cylinders.

The fabricated gel cylinders were incubated in DMEM or 0.1 M NaCl for 3, 5, or 7 days, before analysis of the gel stiffness using a universal testing machine at a speed of 1 mm min^{-1}. At least 3 samples were examined for each test in 3 independent experiments. Stress was determined by the ratio between the applied force and the cross-sectional area of the gel cylinder. Strain was determined by the ratio between the axial elongation and the total length of the gel cylinder. Calculations were performed based on the assumption that the cross-sectional area of the gel cylinder did not change during loading.

Morphing Around Bone: Chicken tibias were acquired from a local supermarket. After all the muscles and tendons were removed from the bone as much as possible, the cleaned bones were kept in NaClO

for 2 days, with the solution being changed twice a day, for complete removal of the superficial organic matrix. The bones were then washed thoroughly with ultrapure water, dehydrated with a gradient series of (50%, 70%, 100%) ethanol, and left to dry.

The horizontally patterned PPy-Alg-PMNF actuators and the bone sample were immersed into a three-electrode cell, as described above, containing DMEM or a 0.1 M NaCl solution. Next, a potential of −0.7 V was applied to the actuator to induce it to morph around the bone and the actuator was kept in this position for 3 days in DMEM or NaCl. Thereafter, potential steps between +0.5 and −0.7 V (each potential for 300 s, 3 cycles) were applied to investigate the attachment of the PPy-Alg-PMNF actuator to the bone.

Alternatively, to allow a more uniform contact of the gel and bone surfaces, the unpatterned PPy-Alg-PMNF actuators were manually wrapped around the bone and held tightly by using yarn. The actuators were then incubated in DMEM or 0.1 M NaCl for 3 days, and thereafter manually removed from the bone. Attachment was assessed by the inability of the actuator to separate from the bone and by the presence of any gel and PMNF-formed minerals onto the bone surface. The presence of gel/minerals on the bone or PPy was assessed using a portable USB microscope and SEM images.

Supporting Information

Supporting Information is available from the Wiley Online Library or from the author.

Acknowledgements

The authors thank Chunxia Du (Dept. Physics, Chemistry and Biology (IFM), Linköping University, Sweden) for her assistance in the cleanroom. Funding: This work was supported by Japanese Society of the Promotion of Science (JSPS) Bridge Fellowship program (BR170502) and KAKENHI (JP20H04534), Swedish Research Council (VR2014-3079), Promobilia (F17603), and China Scholarship Council (201808330454). This work was also supported by bilateral joint research project grant by JSPS (JPJSBP 120 209 923) and STINT, The Swedish Foundation for International Cooperation in Research and Higher Education (MG2019-8171).

Conflict of Interest

The authors declare no conflict of interest.

Data Availability Statement

The data that support the findings of this study are available from the corresponding author upon reasonable request.

Keywords

actuators, biohybrids, mineralization, variable stiffness

Received: September 15, 2021
Revised: November 12, 2021
Published online:

[1] a) R. Baines, S. Freeman, F. Fish, R. Kramer, *Bioinspiration Biomimetics* **2020**, *15*, 025002; b) C. Laschi, B. Mazzolai, M. Cianchetti, *Sci. Rob.* **2016**, *1*, eaah3690; c) S. Miyashita, S. Guitron, S. Li, D. Rus, *Sci. Rob.* **2017**, *2*, eaao4369; d) A. Tonazzini, S. Mintchev, B. Schubert, B. Mazzolai, J. Shintake, D. Floreano, *Adv. Mater.* **2016**, *28*, 10142; e) I. Must, E. Sinibaldi, B. Mazzolai, *Nat. Commun.* **2019**, *10*, 344; f) L. Wang, Y. Yang, Y. Chen, C. Majidi, F. Iida, E. Askounis, Q. Pei, *Mater. Today* **2018**, *21*, 563.

[2] S.-H. Byun, J. Y. Sim, Z. Zhou, J. Lee, R. Qazi, M. C. Walicki, K. E. Parker, M. P. Haney, S. H. Choi, A. Shon, *Sci. Adv.* **2019**, *5*, eaay0418.

[3] a) R. A. Sun Han Chang, J. F. Shanley, M. E. Kersh, B. A. C. Harley, *Sci. Adv.* **2020**, *6*, eabb6763; b) D. Macaya, M. Spector, *Biomed. Mater.* **2012**, *7*, 012001; c) A. R. Short, D. Koralla, A. Deshmukh, B. Wissel, B. Stocker, M. Calhoun, D. Dean, J. O. Winter, *J. Mater. Chem. B* **2015**, *3*, 7818.

[4] a) M. Schaffner, J. A. Faber, L. Pianegonda, P. A. Rühs, F. Coulter, A. R. Studart, *Nat. Commun.* **2018**, *9*, 878; b) D. Rus, M. T. Tolley, *Nature* **2015**, *521*, 467; c) H. Koerner, G. Price, N. A. Pearce, M. Alexander, R. A. Vaia, *Nat. Mater.* **2004**, *3*, 115.

[5] a) Y. Yu, Q. Wang, C. Wang, L. Shang, *Eng. Regen.* **2021**, *2*, 96; b) D. J. Levine, K. T. Turner, J. H. Pikul, *Adv. Mater.* **2021**, *33*, 2007952; c) J. Yu, E. Han, M. A. Hossain, K. Watanabe, T. Taniguchi, E. Ertekin, A. M. van der Zande, P. Y. Huang, *Adv. Mater.* **2021**, *33*, 2007269; d) D. Shah, B. Yang, S. Kriegman, M. Levin, J. Bongard, R. Kramer-Bottiglio, *Adv. Mater.* **2021**, *33*, 2002882.

[6] E. S. Hara, M. Okada, N. Nagaoka, T. Hattori, T. Kuboki, T. Nakano, T. Matsumoto, *ACS Biomater. Sci. Eng.* **2018**, *4*, 617.

[7] a) H. C. Anderson, J. B. Sipe, L. Hessle, R. Dhamyamraju, E. Atti, N. P. Camacho, J. L. Millán, *Am. J. Pathol.* **2004**, *164*, 841; b) L. Hessle, *Proc. Natl. Acad. Sci. USA* **2002**, *99*, 9445.

[8] E. S. Hara, M. Okada, T. Kuboki, T. Nakano, T. Matsumoto, *J. Mater. Chem. B* **2018**, *6*, 6153.

[9] a) T. Osathanon, C. M. Giachelli, M. J. Somerman, *Biomaterials* **2009**, *30*, 4513; b) M. Guan, W. Yao, R. Liu, K. S. Lam, J. Nolta, J. Jia, B. Panganiban, L. Meng, P. Zhou, M. Shahnazari, *Nat. Med.* **2012**, *18*, 456.

[10] a) E. W. H. Jager, E. Smela, O. Inganäs, *Science* **2000**, *290*, 1540; b) E. Smela, *J. Micromech. Microeng.* **1999**, *9*, 1; c) L. Bay, T. Jacobsen, S. Skaarup, K. West, *J. Phys. Chem. B* **2001**, *105*, 8492.

[11] D. Melling, J. G. Martinez, E. W. H. Jager, *Adv. Mater.* **2019**, *31*, 1808210.

[12] a) E. W. Jager, O. Inganäs, I. Lundström, *Science* **2000**, *288*, 2335; b) A. Maziz, C. Plesse, C. Soyer, C. Chevrot, D. Teyssié, E. Cattan, F. Vidal, *Adv. Funct. Mater.* **2014**, *24*, 4851; c) K. Rohtlaid, G. T. M. Nguyen, C. Soyer, E. Cattan, F. Vidal, C. Plesse, *Adv. Electron. Mater.* **2019**, *5*, 1800948.

[13] A. Khaldi, C. Plesse, C. Soyer, E. Cattan, F. Vidal, C. Chevrot, D. Teyssié, in *Proc. ASME 2011 Int. Mechanical Engineering Congress and Exposition. Vol. 2: Biomedical and Biotechnology Engineering; Nanoengineering for Medicine and Biology*, American Society of Mechanical Engineers, New York, **2011**, pp. 755–757.

[14] a) A. Liu, L. Zhao, H. Bai, H. Zhao, X. Xing, G. Shi, *ACS Appl. Mater. Interfaces* **2009**, *1*, 951; b) E. W. Jager, E. Smela, O. Inganäs, *Science* **2000**, *290*, 1540.

[15] T. F. Otero, J. G. Martinez, *Prog. Polym. Sci.* **2015**, *44*, 62.

[16] J.-Y. Sun, X. Zhao, W. R. Illeperuma, O. Chaudhuri, K. H. Oh, D. J. Mooney, J. J. Vlassak, Z. Suo, *Nature* **2012**, *489*, 133.

[17] a) M. C. Darnell, J.-Y. Sun, M. Mehta, C. Johnson, P. R. Arany, Z. Suo, D. J. Mooney, *Biomaterials* **2013**, *34*, 8042; b) F. Vidal, J. F. Popp, C. Plesse, C. Chevrot, D. Teyssie, *J. Appl. Polym. Sci.* **2003**, *90*, 3569.

[18] T. F. Otero, J. M. Sansiñena, *Bioelectrochem. Bioenerg.* **1997**, *42*, 117.

[19] a) A. Fannir, C. Plesse, G. T. Nguyen, F. Vidal, *Smart Mater. Struct.* **2021**, *30*, 025041; b) K. Rohtlaid, G. T. Nguyen, C. Soyer, E. Cattan, F. Vidal, C. Plesse, *Adv. Electron. Mater.* **2019**, *5*, 1800948.

[20] M. Bruchet, A. Melman, *Carbohydr. Polym.* **2015**, *131*, 57.

[21] a) M. Tyagi, J. Pan, E. W. Jager, *Microsyst. Nanoeng.* **2019**, *5*, 44; b) E. Jager, M. Krogh, *WO2004092050*, **2003.**
[22] S. Joshi, K. Rawat, K. C. , V. Rajamohan, A. T. Mathew, K. Koziol, V. K. Thakur, A. S. S. Balan, *Appl. Mater. Today* **2020**, *18*, 100490.
[23] a) P. K. Kreeger, J. W. Deck, T. K. Woodruff, L. D. Shea, *Biomaterials* **2006**, *27*, 714; b) D. S. Garske, K. Schmidt-Bleek, A. Ellinghaus, A. Dienelt, L. Gu, D. J. Mooney, G. N. Duda, A. Cipitria, *Tissue Eng., Part A* **2020**, *26*, 852; c) P. M. George, A. W. Lyckman, D. A. LaVan, A. Hegde, Y. Leung, R. Avasare, C. Testa, P. M. Alexander, R. Langer, M. Sur, *Biomaterials* **2005**, *26*, 3511; d) K. J. Gilmore, M. Kita, Y. Han, A. Gelmi, M. J. Higgins, S. E. Moulton, G. M. Clark, R. Kapsa, G. G. Wallace, *Biomaterials* **2009**, *30*, 5292; e) D. Khodagholy, T. Doublet, M. Gurfinkel, P. Quilichini, E. Ismailova, P. Leleux, T. Herve, S. Sanaur, C. Bernard, G. G. Malliaras, *Adv. Mater.* **2011**, *23*, H268; f) X. Song, C. Liang, H. Gong, Q. Chen, C. Wang, Z. Liu, *Small* **2015**, *11*, 3932; g) A. Fahlgren, C. Bratengeier, A. Gelmi, C. M. Semeins, J. Klein-Nulend, E. W. Jager, A. D. Bakker, *PLoS One* **2015**, *10*, e0134023; h) A. Gelmi, M. K. Ljunggren, M. Rafat, E. Jager, *J. Mater. Chem. B* **2014**, *2*, 3860.
[24] a) A. Punning, M. Kruusmaa, A. Aabloo, *Sens. Actuators, A* **2007**, *133*, 200; b) C. Bohn, S. Sadki, A. B. Brennan, J. R. Reynolds, *J. Electrochem. Soc.* **2002**, *149*, E281.
[25] T. F. Otero, M. T. Cortes, *Adv. Mater.* **2003**, *15*, 279.
[26] K. Kaneto, E. Jager, G. Alici, H. Okuzaki, in *Electromechanically Active Polymers. Polymers and Polymeric Composites: A Reference Series* (Ed: F. Carpi), Springer, Cham, Switzerland **2016**, https://doi.org/10.1007/978-3-319-31767-0_16-1
[27] J. M. Suski, M. Lebiedzinska, A. Wojtala, J. Duszynski, C. Giorgi, P. Pinton, M. R. Wieckowski, *Nat. Protoc.* **2014**, *9*, 312.
[28] H. Miyajima, T. Matsumoto, T. Sakai, S. Yamaguchi, S. H. An, M. Abe, S. Wakisaka, K. Y. Lee, H. Egusa, S. Imazato, *Biomaterials* **2011**, *32*, 6754.